Solar Energy Materials & Solar Cells 257 (2023) 112350

Contents lists available at ScienceDirect

Solar Energy Materials and Solar Cells

journal homepage: www.elsevier.com/locate/solmat

Thermochromic glass laminates comprising W/VO_2 nanoparticles obtained by wet bead milling: An in-depth study of the switching performance

Lavinia Calvi [a,b,c], Ryan van Zandvoort [d,e], Luc Leufkens [d,e], Janique F.B. Hupperetz [d,e], Roberto Habets [d,e], Daniel Mann [d,e], Nicole Meulendijks [d,e], Marcel A. Verheijen [f,g], Ken Elen [a,b,c], An Hardy [a,b,c], Marlies K. Van Bael [a,b,c], Pascal Buskens [a,d,e,*]

[a] Design and Synthesis of Inorganic Materials (DESINe), Institute for Materials Research, Hasselt University, Agoralaan Building D, 3590, Diepenbeek, Belgium
[b] IMEC vzw, IMOMEC Associated Laboratory, Wetenschapspark 1, 3590, Diepenbeek, Belgium
[c] EnergyVille, Thor Park 8320, 3600, Genk, Belgium
[d] The Netherlands Organisation for Applied Scientific Research (TNO), High Tech Campus 25, 5656 AE, Eindhoven, the Netherlands
[e] Brightlands Materials Center, Urmonderbaan 22, 6167 RD, Geleen, the Netherlands
[f] Department of Applied Physics, Eindhoven University of Technology, 5600 MB, Eindhoven, the Netherlands
[g] Eurofins Materials Science, High Tech Campus 11, 5656 AE, Eindhoven, the Netherlands

A B S T R A C T

The switching performance of W/VO_2 nanoparticles in thermochromic glass laminates was investigated. W/VO_2 powder was prepared, and displayed a phase transition temperature and switching enthalpy of 20.9 °C and 37.5 ± 0.2 J g^{-1}, respectively. Using wet bead milling, the particle size was reduced from 24 ± 2 μm to 120 ± 10 nm. In the same process, the switching enthalpy decreased to 18.2 ± 0.6 J g^{-1} due to partial loss of crystallinity. The kinetics of the structural phase transition were studied using Friedman's differential isoconversional method. This demonstrated that the activation energy $|E_\alpha|$ was inversely proportional to the square of the difference between the material's temperature and the critical switching temperature T_0, pointing out that nucleation kinetics were determining the rate. Furthermore, $|E_\alpha|$ decreased upon milling, and kinetic asymmetry was induced. The milled nanoparticles were compounded with PVB to produce thermochromic films, which were applied for laminating glass plates. The impact of nanoparticle size and concentration on the resulting optical properties of the laminate, viz. solar transmission and solar modulation, was studied in detail. The highest solar modulation obtained was 9.4%. The results obtained in this study are of direct importance for the application in smart windows, showing that (i) the W/VO_2 particle size needs to be ≤ 100 nm to avoid excessive haze, (ii) both powder production and bead milling require further process optimization to minimize functional performance losses, and (iii) T_0 should be set about 3 °C lower to ensure a sufficiently fast switch at the temperature of choice.

1. Introduction

Monoclinic vanadium dioxide VO_2 (M) is an interesting material because of its thermochromic properties, which can be tailored for a range of applications such as smart windows [1], solar absorbers [2], sensors [1], electronic devices [1], actuators [1], power meters or thermometers [1], optical and holographic devices [1], ionic gratings [3], improved computational approaches [3], and new ultrafast microscopy techniques [3]. Depending on the application the phase transition temperature (T_0), which is normally 68 °C, is adjusted by integrating intrinsic point defects, dopants such as W^{6+} or strain into the crystal structure [4]. At T_0 VO_2 undergoes a structural phase transition (SPT) from monoclinic VO_2 (M) to rutile VO_2 (R), which is accompanied by a first order metal-insulator transition (MIT). The transition leads to changes in electronic and optical properties of the material: VO_2 (M) is a semiconductor with high transmission for solar infrared radiation (solar-IR), whilst VO_2 (R) is an electrical conductor that absorbs solar-IR. We focus on the integration of VO_2 in smart thermochromic windows for energy savings. Recent publications in the field of VO_2-based smart windows focused on VO_2 coatings on flexible substrates [5], synthesis of VO_2 nanoparticles [6], nanocomposite coatings [7], nanocomposite films [8,9] and multifunctional thermochromic coatings [10,11]. Recent progress in the field of VO_2-based materials for smart windows is reviewed by Arubas et al. [12] and Long and Gao [13]. For application in smart windows, T_0 needs to be lowered to 15–25 °C, depending on the local climate and building characteristics, for optimum energy savings [14,15]. By introducing W^{6+} in small amounts between 1 and 3.5 at-%, T_0 can be tailored between 68 °C and −10 °C [16–18], based on a

* Corresponding author. Design and Synthesis of Inorganic Materials (DESINe), Institute for Materials Research, Hasselt University, Agoralaan Building D, 3590, Diepenbeek, Belgium.
E-mail address: pascal.buskens@tno.nl (P. Buskens).

https://doi.org/10.1016/j.solmat.2023.112350
Received 3 February 2023; Received in revised form 12 April 2023; Accepted 25 April 2023
Available online 5 May 2023

distortion of the VO_2 lattice structure and integration of defects. The switching enthalpy ΔH is the heat which is released and absorbed during the first order phase transition from VO_2 (M) to VO_2 (R) and *vice versa* and directly relates to the functional performance of the material (magnitude of the switch ΔT_{sol}, *vide infra*).

Integrating VO_2 as nanoparticles in coatings and polymer films is accompanied by challenges such as particle distribution in the matrix material and potential agglomeration, chemical compatibility with polymers and other coating or film materials, and potential oxidation during processing of coatings (*e.g.* thermal anneal) or polymer nanocomposites (*e.g.* compounding, extrusion, lamination). Additionally, at high VO_2 concentrations and film thicknesses, the luminous transmittance (T_{lum}, 380–780 nm) is low [19–21], since a large portion of the visible light is either absorbed or reflected [22,23]. Therefore, achieving a high modulation of solar energy (ΔT_{sol}, 380–2500 nm) combined with a high T_{lum} is challenging as increasing ΔT_{sol} generally leads to a decrease in T_{lum} and *vice versa* [21,24–28]. Granqvist and co-workers proposed the concept of nanothermochromic films to simultaneously increase both parameters [24,29–33]. Nanoparticles are required to have a size below 100 nm to avoid visible light scattering, random distribution of particles within the film (to avoid agglomeration) and high purity and crystallinity of the material are needed to ensure an optimum switching performance [31,34–36].

For the production of VO_2 (M) nanoparticles, VO_2 (M) powders are prepared as bulk material, and the particle size is subsequently reduced by wet bead milling. Shi et al. [18] synthesised W/VO_2 powder starting from vanadyl sulphate hydrate, ammonium bicarbonate and sodium tungstate as reagents in deionised water. A slurry of the W/VO_2 powder in xylene was subjected to a planetary ball mill at 650 rpm for 30–60 min to reduce the particle size. The resulting particles were subsequently embedded in an acrylic resin to form a thermochromic film. The 2 wt-% W-doped sample which was milled for 30 min displayed an average particle size of 275 nm. The acrylic films reached a maximum transmission of around 60% in the visible, with a change in transmittance of around 18% at a wavelength of 1600 nm upon switching. Increasing the milling time to 1 h resulted in the peak temperature slightly increasing from 24.2 °C to 24.7 °C and the enthalpy decreasing from 21.3 J g^{-1} to 7.4 J g^{-1}. Additionally, the intensity of the XRD peaks decreased upon milling, suggesting that the procedure reduced the material's crystallinity.

Lu et al. [37] synthesised W/VO_2 with the same reagents used by Shi et al. [18] and a similar preparation procedure. The W/VO_2 powder was dispersed in a mixture of butyl acetate and 3-methacryloxypropyltrimethoxysilane, and bead milled for 10 h at a speed of 3000 rpm using 0.3 mm zirconia beads. This resulted in the formation of W/VO_2 particles with an average size of 200 nm. Their results illustrated both a decrease in switching enthalpy upon milling and a lowered XRD peak intensity. After centrifugation and other processing steps, the W/VO_2 nanoparticles were dispersed in polysiloxane oligomers to obtain coatings with varying solid content. Coatings with three different W/VO_2 contents were realized (1, 4 and 10 wt-%) of which the transmittance at 550 nm decreased from 89% (1 wt-%) to 59% (10 wt-%) with increasing concentration of W/VO_2. The difference in transmittance at 1600 nm upon switching increased from around 8% for the 1 wt-% coating to 20% for the 10 wt-% coating.

Takai et al. [38] milled V_2O_5 and paraffin wax with varying weight ratios (30:1–10:1), the milling time was varied between 3 h and 10 h and doping was carried out by addition of 1 at-% of Cr_2O_3, MoO_3 or WO_3 during the milling process. Milling was performed under air using a planetary mill with 15 mm and 5 mm yttria-stabilized zirconia beads. After milling the V_2O_5 for 3 h (without doping) the produced VO_2 has a peak switching temperature of 53.0 °C with an enthalpy of 21.6 J g^{-1}. Milling in the presence of WO_3 apparently resulted in poor dopant integration as the shift in the switching temperature is only of a few degrees. Unfortunately, there are no data available on the optical properties of the resulting material in coatings or films.

Wang et al. [39] synthesised VO_2 by bead milling of V_2O_5 with activated carbon at a rotor speed of 1425 rpm up to 4 h. W/VO_2 samples were prepared by adding tungstic acid in different molar ratios to V_2O_5 to achieve 1, 2 and 3 at-% doping. After washing and drying, the samples were heated to 300 °C for 4 h *in vacuo*. The W/VO_2 powders were then dispersed in ethanol comprising dissolved polyvinyl butyral (PVB), and subsequently the dispersion was cast onto a microscope slide and dried. The sample with 2 at-% W-doping displayed an average particle size of 43 nm, and a switching temperature of 30.4 °C. The switching enthalpy was not reported. The PVB film comprising W/VO_2 had a thickness of 1.4 μm and displayed a transmittance of around 56% at 550 nm and a modulation of around 30% at 1600 nm. The corresponding ΔT_{sol} is 9.68% and the T_{lum} is 44.18%.

Although the preparation of W/VO_2 nanoparticles by bead milling of powders has been reported, a systematic study on the impact of bead milling on the thermodynamics and kinetics of the SPT of these particles is still lacking. This is of direct importance for the application in smart windows, since the thermodynamics directly impact ΔT_{sol}, and the kinetics dictate whether the switch occurs sufficiently fast at the temperature of choice to avoid further heating of the building's interior before completely switching and blocking the solar IR radiation. In practice, this implies that the switch should be complete within a period of roughly 30 min. To date, only the thermodynamics and switching kinetics of the SPT of VO_2 and W/VO_2 powders and milled undoped VO_2 nanoparticles have been systematically studied by our group [16,40]. Furthermore, a systematic study on the relationship between the thermodynamics and kinetics of the SPT of W/VO_2 nanoparticles and the functional performance of thermochromic PVB laminated glass comprising such particles has not yet been achieved. Here, we report an in-depth study on the thermodynamics and kinetics of the SPT of W/VO_2 nanoparticles of various sizes obtained by wet bead milling. Furthermore, we relate these characteristics and the size of the nanoparticles to the functional performance of thermochromic glass laminates comprising them.

2. Experimental section

2.1. Preparation of vanadyl oxalate solution

The vanadyl oxalate solution is prepared at 80 °C by slowly adding vanadium(V) oxide (V_2O_5, 300.0 g, 1.649 mol; 99.6%, Sigma-Aldrich) to a stirred slurry of oxalic acid ($C_2H_2O_4$, 638.55 g, 7.095 mol; 98%, Sigma-Aldrich) in Milli-Q water (700.0 g). Note: V_2O_5 is added slowly due to gases evolving during the reaction. After the complete addition of V_2O_5, 2-propanol (IPA) (85.0 g; 99.8%, Sigma-Aldrich) and Milli-Q water (400.0 g) are added. The solution is stirred for 1 h at 80 °C. After cooling to room temperature, the solution is further diluted using IPA (700.0 g) to obtain a vanadyl oxalate concentration of 0.875 mol kg^{-1}. The synthesis route is illustrated in Fig. 1a.

2.2. Preparation of tungsten solution

The tungsten solution was prepared by dissolving tungsten hexachloride (WCl_6, 10 g, 99.9+%, Acros Organics) in IPA (300 g) to obtain a W^{6+} concentration of 0.084 mol kg^{-1}.

2.3. Synthesis of W/VO_2 powder

The vanadyl oxalate solution with 2 at-% W is prepared by adding all of the tungsten solution prepared in section 2.2. to the vanadyl oxalate solution prepared in section 2.1. The resulting mixture is stirred for 16 h at room temperature. The solvent is subsequently removed using a rotary evaporator, and the resulting blue powder is crushed using a mill with a sieve of 2 mm (Polymix PX-MFX 90 D). The resulting fine powder (204 g) is then annealed in a rotary tube furnace (Carbolite Gero HTR 1100) equipped with a quartz tube (Fig. S1), in analogy to a previously

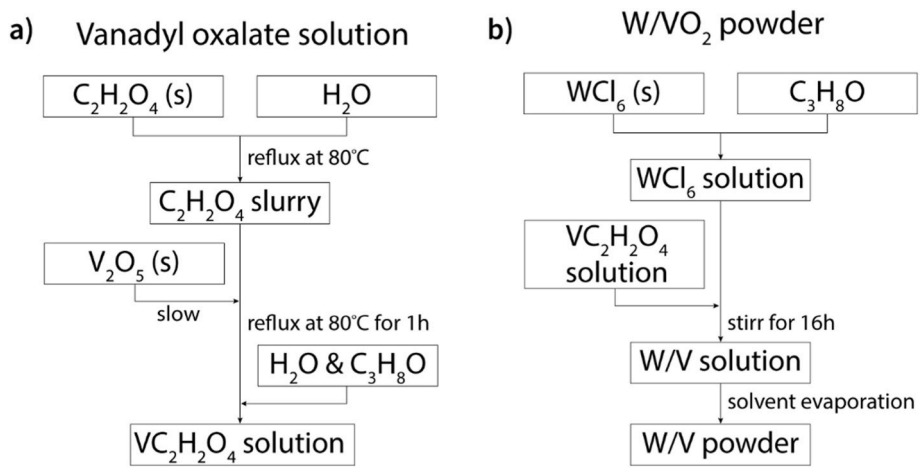

Fig. 1. a) Synthesis route of vanadyl oxalate solution, b) synthesis route of the W/V powder which is converted to W/VO_2 in a thermal anneal process.

reported procedure [16]. The powder product is characterised and used for bead milling experiments. The synthesis and processing route is illustrated in Fig. 1b.

2.4. Bead milling procedure

The W/VO_2 powder obtained after thermal anneal in the tube furnace (section 2.3.) is sieved with an aperture of 100 μm (VWR). The remaining material is crushed using a mortar and pestle, and subsequently sieved using the same procedure. The W/VO_2 powder (120 g) is added to IPA (270 g) and sonicated in an ultrasonic bath for 15 min to yield a slurry suited for addition to the bead mill. The milling is carried out using two different chambers: firstly, the Bühler PML 2 is fitted with a Sentex S2 milling chamber with SiC lining and stainless steel rotor having an internal volume of 600 mL (Fig. S2a). The milling chamber is pre-filled with zirconium oxide beads (480 mL, 1.87 kg, 80% of chamber volume, yttrium stabilized, 0.65 mm, Bühler, Draison®YUP) and IPA (410 g). The VO_2 slurry is slowly added to the milling chamber at low rpm and low pump speed. The start content is 15 wt-% of VO_2 during the milling. Milling is carried out at 1500 rpm and 40% pump power till 2000 $kWht^{-1}$ milling energy was reached. The milled W/VO_2 slurry is slowly pumped out of the system and collected in a glass jar. After cleaning of the system with water, the system is fitted with a Micro-Media™ L milling chamber, having an internal volume of 70 mL (Fig. S2b). The milling chamber was pre-filled with zirconium oxide beads (56 mL, 208 g, 80% of chamber volume, yttrium stabilized, 0.2 mm, Bühler, Draison®YUP) and IPA (150 g). After the slow addition of the slurry and IPA (300 g) the total W/VO_2 content was 10 wt-%. The rotor speed was initially set to 1500 rpm and the pump power to 40%. Throughout the milling the rotor speed was increased to 3000 rpm (Table S2). During milling the dispersion was kept at a temperature below 35 °C using water cooling. The system was continuously flushed with nitrogen to prevent oxidation of W/VO_2. Samples were taken every 3000 $kWh{\cdot}t^{-1}$ milling energy. Material was dried in a vacuum oven at 40 °C to obtain a powder suited for differential scanning calorimetry (DSC), X-ray diffraction (XRD), transmission electron microscopy (TEM) and scanning electron microscopy (SEM) analyses.

2.5. Fabrication of W/VO_2-PVB masterbatch

PVB (35.0 g, >99%; BUTACITE® BF1400 PVB flake, Du Pont) is dissolved in ethanol (465.0 g, 99.8%, Sigma-Aldrich) to make a 7 wt-% stock solution. The milled W/VO_2 (10 wt-% in IPA, 1.0 g) nanoparticles are dispersed in ethanol (10.0 g) and then PVB stock solution (141.4 g) is added. The resulting mixture is stirred. After stirring the mixture is dried in an oven at 50 °C to allow the solvents to evaporate, and the resulting W/VO_2-PVB masterbatch was obtained with a W/VO_2 concentration of 1 wt-%. Thermogravimetric analysis (TGA) was performed to confirm the final concentration of W/VO_2 in the masterbatch (10 $°C{\cdot}min^{-1}$ up to 600 °C).

2.6. Production of thermochromic films and glass laminates

The microcompounder 15HT (Explore instruments BV) is used to extrude strands with varying W/VO_2 concentration (Fig. S3). The 1 wt-% $W\text{-}VO_2$ masterbatch is diluted to 0.08 – 0.005 wt-% W/VO_2 comprising PVB strands consisting of blank PVB and OXSOFT 3G8 (>97%, triethylene glycol-di(2-ethylhexanoate), OXEA) in a 70/30 wt ratio. The compounding is carried out at 180 °C, initially with a slow addition at 30 rpm and then increased to 150 rpm for two to 5 min, before opening of the valve to pull the pigmented strands.

Thermochromic laminates are produced using a Lotus hot press at 150 °C. The W/VO_2-PVB strand is evenly distributed between two glass plates (Pilkington Optiwhite, 3.8 mm) and placed in the hot press (Fig. S4). Initially 0.5 bar pressure is applied for 2 min to heat up the stack and then the pressure is gradually increased to 1 bar for 2 min. The thickness of the PVB interlayer was measured using a Mitutoyo ID-H0530 543 series, which has an accuracy of 0.1 μm.

2.7. Procedure and data collection for the kinetics study

DSC was carried out on a Discovery DSC (TA Instruments) using Tzero aluminium pans containing 20 mg of dried sample. All the samples were subjected to the following six heating and cooling rates: 1.5, 5, 7.5, 10, 15 and 20 $°C{\cdot}min^{-1}$. Before data collection all DSC pans were subjected to 4 cycles of heating and cooling at 20 $°C{\cdot}min^{-1}$ from −60 to 120 °C to ensure that the samples were completely dry. After this procedure, the sample mass was determined again. The collected data were analysed with TRIOS software v5.1 and processed in accordance with Friedman's isoconversional method, which is discussed in section 3.1. The enthalpy calculation is carried out using the peak integration with respect to time within the TRIOS software. Calibration checks and calibrations were carried out frequently to ensure the measurements are reliable. Specifically, following calibrations were carried out: the baseline, the temperature, heat flow and standard heat capacity calibrations. The baseline calibration was carried out with an empty cell in the temperature range between −90 and 400 °C at a heating rate to 20 $°C{\cdot}min^{-1}$ and this was repeated by placing a sapphire without the pan on both sample and reference side. Heat flow and temperature calibration were carried out with indium at a heating rate of 10 $°C{\cdot}min^{-1}$. The standard heat capacity calibration used sapphire from −80 to 400 °C at a heating rate of 20 $°C{\cdot}min^{-1}$.

2.8. Characterization techniques

Laser diffraction measurements were carried out to determine the size of the dispersed W/VO_2 nanoparticles using the Mastersizer 3000 from Malvern Panalytical. 15 drops of dispersion were added to 15 mL of IPA, and the ultrasonic tip was used for 2 min at 10 Hz (about 800 J). The D10, D50 and D90 represent the percentile of the particle size, therefore the cumulative ascending size of 10% of the sample (D10). X-ray diffraction (XRD) measurements to determine the composition of the W/VO_2 particulate materials were carried out on a Bruker D2 PHASER. Discovery DSC (TA Instruments) was used for the DSC measurements. Scanning transmission electron microscopy – energy dispersive X-ray (STEM-EDX) analyses were performed using a probe-corrected JEOL ARM 200F operated at 200 kV, equipped with a 100 mm2 SDD EDS detector. The method used was High Angle Annular Dark Field (HAADF) STEM, and EDX, spot 3 C. The cross-sectional TEM sample was prepared using microtomy sectioning, using a Leica Reichert Ultracut S. The volume fraction of the VO_2 was approximated to 0.0007 vol-% for 0.03 wt-% since VO_2 has a much higher density than PVB. Therefore, coupes were kept relatively thick (~500 nm) in order to ensure the coupes would contain several VO_2 clusters within the field-of-view. The TENEO Scanning Electron Microscope (SEM) was used for obtaining images of the milled W/VO_2 particulate materials. The size was determined using Martin's diameter method by measuring the length and width of each particle in ImageJ. [41] The measurements of the thermochromic coatings were carried out using a Perkin Elmer Lambda 750 UV–vis–NIR spectrometer equipped with a temperature-controlled module manufactured by OMT Solutions B.V. for measuring transmission at temperatures between −10 °C and 90 °C (Fig. S5).

3. Results and discussion

3.1. Preparation and characterization of W/VO_2 powder and nanoparticles

W/VO_2 powder with 2 at-% W was prepared by combining a vanadyl oxalate solution and a solution of WCl_6 in the appropriate ratio. The blue vanadyl oxalate solution was prepared by chemical reduction of V_2O_5 with an excess of oxalic acid. After combining both solutions and removal of solvents and other volatiles *in vacuo*, the remaining blue-green powder was grinded and sieved, and subsequently converted to W/VO_2 in a multistep thermal anneal process using a rotating tube furnace. XRD analysis demonstrated the presence of a mixture of VO_2 (M) and VO_2 (R) at room temperature (Fig. 2a). DSC analysis confirmed that both VO_2 (M) and VO_2 (R) were present between 10 and 30 °C (Fig. 2b). In the DSC of the non-milled W/VO_2 powder and milled particulate materials (Fig. 2b) the temperature range of the heating and cooling curve largely overlaps. In case of a single pure W/VO_2 species, such overlap would be thermodynamically forbidden. This leads to the conclusion that the W/VO_2 powder and the particulate materials produced do not consist of one switching species, but of a mixture of W/VO_2 species with different particle size, W-concentration and W-distribution within the particles, which switch between 10 and 30 °C. Consequently, the XRD analysis performed at room temperature (20 °C) displays a mixture of monoclinic and rutile W/VO_2 (Fig. 2a). The XRD characteristic peaks at 27.8° and 27.9° were shifted by 0.1° compared to undoped VO_2 because the W-doping caused a distortion in the VO_2 crystal lattice (Fig. 2a). For magnified XRDs of the milled particles, see Fig. S6. From DSC analysis, we obtained switching temperatures at 50% conversion ($T_{\alpha = 0.50}$) of 20.9 °C and 17.1 °C for the switch from VO_2 (M) to VO_2 (R) and *vice versa* (Fig. 2b). The difference in both switching temperatures is fairly small, viz. 3.8 °C, and corresponds to the hysteresis width. Furthermore, the DSC signals are rather broad, which is illustrated by the large difference of 20.86 °C between $T_{\alpha = 0.50}$ and the temperature at the start of switch ($T_{\alpha = 0.02}$ = 0.04 °C, Table 2, *vide infra*). Latter corresponds to the hysteresis gradient. In addition to $T_{\alpha = 0.50}$ and ΔH, also these hysteresis characteristics influence the performance of the material in smart window applications [42,43]. This lowering of the switching temperature from 68 °C to near room temperature confirmed the successful integration of W^{6+} in the VO_2 crystal lattice. The switching enthalpy (ΔH) was 37.5 ± 0.2 J g^{-1} (Fig. 2b), which is lower than typical switching enthalpies reported for undoped VO_2 powders [16,40], and in the same range as values previously reported for W-doped VO_2 powders with similar switching temperature (30.7 J g^{-1}) [44].

The W/VO_2 powder was then milled in a two-step procedure to yield particles of a size around 100 nm. At different stages during the milling process, samples were taken and analysed by XRD, DSC, SEM and laser diffraction. With progressive milling, we observed by SEM analyses (Fig. 3c–f) that the particle size in dry state decreases from >20 μm for the non-milled powder to 0.5–3 μm, 0.5–1.5 μm and <0.4 μm for the samples obtained at a milling energy of 2143 kWh·t^{-1}, 11000 kWh·t^{-1} and 17000 kWh·t^{-1}, respectively. We also determined the size of the particles in liquid dispersion using laser diffraction. Fig. 3a illustrates that the particle size decreases and that the size distribution becomes narrower upon milling. The D90 sizes (Fig. 3b) of the milled particles were 24 ± 2 μm (166 kWh·t^{-1}), 3.14 ± 0.08 μm (2143 kWh·t^{-1}), 0.52 ± 0.03 μm (11000 kWh·t^{-1}) and 0.12 ± 0.01 μm (17000 kWh·t^{-1}). These values were in reasonable agreement with the sizes obtained by SEM. As determined by DSC, ΔH decreased upon progressive milling from 37.5

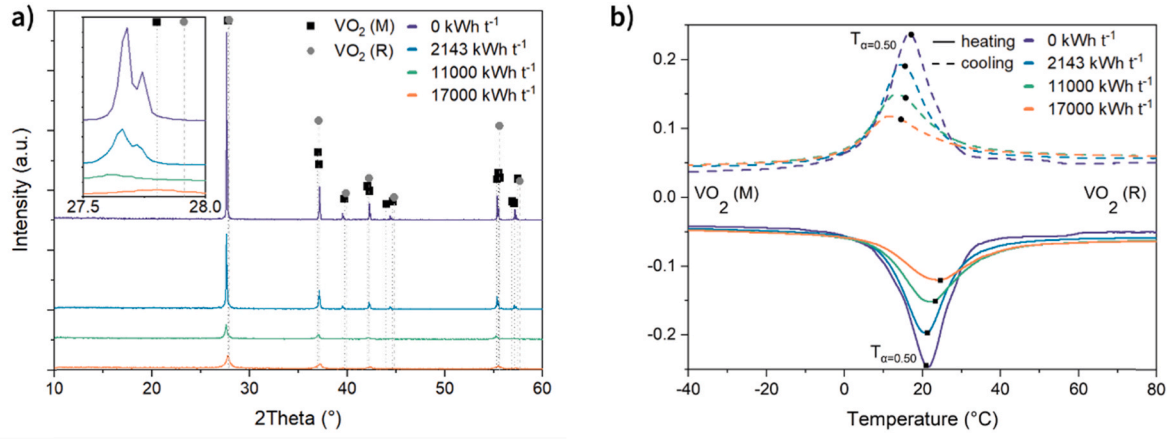

Fig. 2. a) XRD pattern of the non-milled (0 kWh·t^{-1}) and milled W/VO_2 particulate materials (2143 kWh·t^{-1}, 11000 kWh·t^{-1} and 17000 kWh·t^{-1}), phases identified VO_2 (M) JCPDS 65–4795 and VO_2 (R) JCPDS PDF 73–2362, b) DSC of non-milled (0 kWh t^{-1}) W/VO_2 powder and milled particulate materials (2143 kWh·t^{-1}, 11000 kWh·t^{-1} and 17000 kWh·t^{-1}) obtained at a heating rate of 5 °C·min^{-1}.

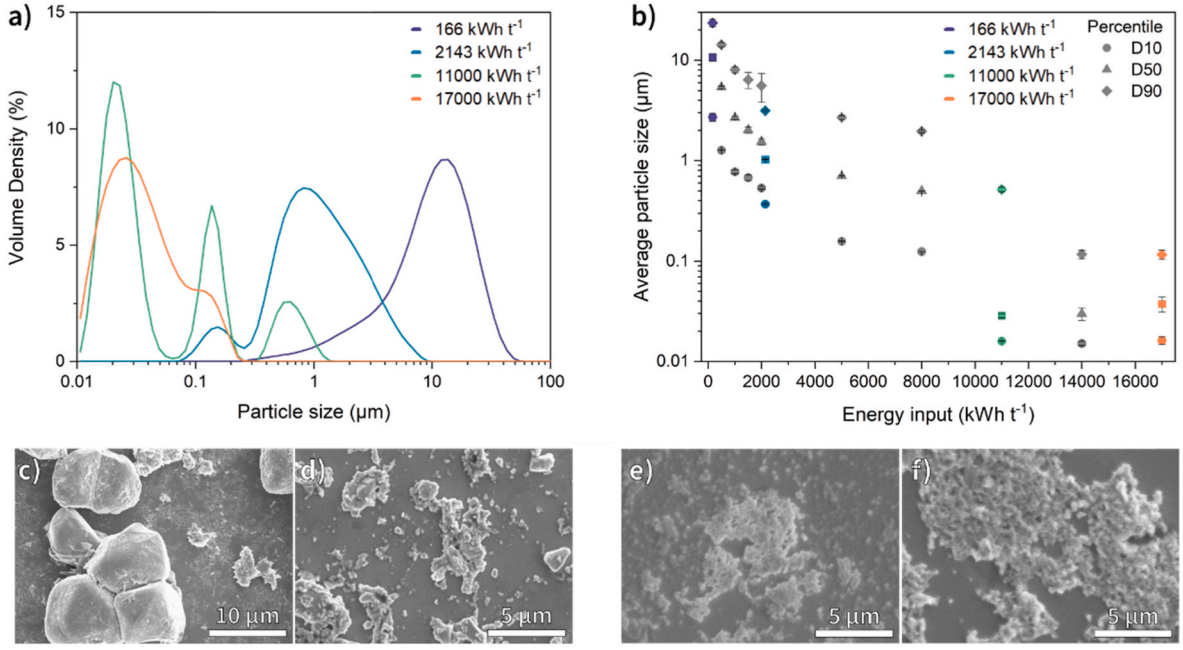

Fig. 3. a) Particle size distribution of the non-milled (166 kWh·t^{-1}) and milled W/VO_2 particulate materials (2143 kWh·t^{-1}, 11000 kWh·t^{-1} and 17000 kWh·t^{-1}) dispersed in IPA and analysed by laser diffraction, b) particle size of the W/VO_2 particulate materials analysed in IPA using laser diffraction at different percentiles (D10, D50 and D90) for a range of milling energy inputs, c) SEM image of non-milled W/VO_2 powder, d) SEM image of milled W/VO_2 particulate material at 2143 kWh·t^{-1} energy input, e) SEM image of milled W/VO_2 particulate material at 11000 kWh·t^{-1} energy input and f) SEM image of milled W/VO_2 particulate material at 17000 kWh·t^{-1} energy input.

± 0.2 J g^{-1} (non-milled) to 29.8 ± 0.3 J g^{-1} (2143 kWh·t^{-1}), 25.8 ± 0.4 J g^{-1} (11000 kWh·t^{-1}) and 18.2 ± 0.6 J g^{-1} (17000 kWh·t^{-1}) for the switch from W/VO_2 (M) to W/VO_2 (R) (Table 1). This decrease of Δ*H* is most likely due to a loss in crystallinity during bead milling. This is supported by the gradually decreasing peak intensity in the XRDs of materials upon progressive milling (Fig. 2a), and in agreement with previously reported observations for undoped VO_2 nanoparticles obtained by bead milling [40]. The XRD shows no signs of crystalline V_2O_5 formation, which suggests that oxidation of W/VO_2 does not occur (Fig. 2a).

Furthermore, we observed an increase in the switching temperature at 2% conversion ($T_{\alpha = 0.02}$) for the switch from W/VO_2 (M) to W/VO_2 (R) and an increase in $T_{\alpha = 0.02}$ for the switch from W/VO_2 (R) to W/VO_2 (M). $T_{\alpha = 0.02}$ gradually increases from 0.04 °C (non-milled) to 0.64 °C (17000 kWh·t^{-1}) for the switch from W/VO_2 (M) to W/VO_2(R) and from 41.36 °C (non-milled) to 47.59 °C (17000 kWh·t^{-1}) for the switch from W/VO_2 (R) to W/VO_2 (M).

3.2. Thermokinetic analysis of milled W/VO_2 particulate materials

In previous studies the kinetics of undoped and W-doped VO_2 powders (1–3.5 at-%) and undoped VO_2 nanoparticles were investigated using Friedman's differential isoconversional method. [16,40] These studies showed that the activation energy of the SPT was infinitely high at T_0 and decreased with increasing difference between the material's temperature and T_0. Furthermore, the activation energy was similar for the SPT from VO_2 (M) to VO_2 (R) and *vice versa* for undoped VO_2 powder and VO_2 powders with up to 2 at-% W as dopant (kinetically symmetric). VO_2 powders with more than 2 at-% W displayed a kinetic asymmetry with a higher activation energy for the SPT from W/VO_2 (R) to W/VO_2 (M) [16,40]. Progressive milling of undoped VO_2 powder resulted in a decrease in activation energy for both SPTs, albeit that the activation energy for the SPT from VO_2 (R) to VO_2 (M) dropped faster which induced a kinetic asymmetry [16,40].

Table 1
Average enthalpy for all DSC heating and cooling rates (1.5, 5, 7.5, 10, 15 and 20 °C·min^{-1}) of the W/VO_2 powder and particulate materials obtained by milling at different milling energy inputs.

Bead milling energy input (kWh·t^{-1})	D90 particle size (μm)	Average enthalpy Δ*H* (J·g^{-1})	
		W/VO_2 (M) to W/VO_2 (R)	W/VO_2 (R) to W/VO_2 (M)
0	24 ± 2	37.5 ± 0.2	36.6 ± 0.3
2143	3.14 ± 0.08	29.8 ± 0.3	29.1 ± 0.6
11000	0.52 ± 0.03	25.8 ± 0.4	24.6 ± 0.7
17000	0.12 ± 0.01	18.2 ± 0.6	16.5 ± 0.7

Table 2
Temperature at 2% and 50% conversion of the non-milled W/VO_2 powder obtained by DSC analysis using a heating/cooling rate of 5 °C·min^{-1} and activation energy at |ΔT| = 2.5 °C of the non-milled and milled W/VO_2 powders.

Bead milling energy input (kWh·t^{-1})	$T_{\alpha = 0.02}$ (°C)		$T_{\alpha = 0.50}$ (°C)		Activation energy E_α (kJ·mol^{-1})	
	W/VO_2 (M) to W/VO_2 (R)	W/VO_2 (R) to W/VO_2 (M)	W/VO_2 (M) to W/VO_2 (R)	W/VO_2 (R) to W/VO_2 (M)	W/VO_2 (M) to W/VO_2 (R)	W/VO_2 (R) to W/VO_2 (M)
0	0.04	41.36	20.87	17.12	668	676
2143	1.22	49.47	21.21	15.57	404	433
11000	1.06	54.21	23.26	15.72	490	297
17000	0.69	47.59	24.55	14.54	502	290

The applied Friedman differential isoconversional method [45,46] was detailed in previous reports. [16,40] In this study only the main equations used will be introduced.

$$-R \ln\left(\frac{d\alpha}{dt}\right)_{\alpha,i} = -R \ln(A_\alpha f(\alpha)) + \frac{E_\alpha}{T_{\alpha,i}} \quad (1)$$

In Equation (1), *A* is a pre-exponential factor (temperature independent), *E* is the activation energy of the SPT, *R* is the gas constant, *T* is temperature, *f(α)* is the reaction model and *α* is the degree of conversion

($0 \leq \alpha \leq 1$). Lastly, i indicates the different heating and cooling rates applied in the DSC analyses. Equation (1) is used for establishing the Friedman plot in which $-R\ln(d\alpha/dt)$ is plotted as function of T^{-1} and the activation energy of the SPT equals the gradient of the tangent at that point. E_α corresponds to the free energy barrier for the nucleus formation (ΔG^*). Assuming the nucleus is spherical for homogeneous nucleation, ΔG^* can be defined in the following manner: [47]

$$\Delta G^* = \frac{16\pi\sigma^3 T_0^2}{3(\Delta H)^2(\Delta T)^2} = \frac{A}{(\Delta T)^2} \tag{2}$$

T_0 is the critical temperature (where the switch is infinitely slow), ΔH is the phase transition enthalpy and σ is the surface energy of the nucleus. These parameters are combined into one integrated constant A, as these are material constants. $\Delta T = T - T_0$ for heating and $\Delta T = T_0 - T$ for cooling, where T is the material temperature. The value of T_0 is taken at a conversion of 2% and referred to as $T_{\alpha = 0.02}$. E_α depends on α [45], and therefore the constant value of $\alpha = 0.50$ is used in our study as here the nucleation is considered homogenous. The extent of conversion equals the fractional enthalpy of the DSC peak, defining the nucleation rate [46].

$$\frac{d\alpha}{dt} = \frac{dH}{A_T dt} \tag{3}$$

Where H is the enthalpy of the phase transition, A_T is the area under the entire thermogram. By combining equation (2) and equation (1) the following relationship is derived:

$$-R\ln\left(\frac{d\alpha}{dt}\right) = -R\ln(\omega_0) + \frac{16\pi\sigma^2}{3(\Delta H)^2} \bullet \frac{T_0^2}{(\Delta T)^2 T} \tag{4}$$

Using equation (4) and the excel built-in solver the dataset was used to fit Friedman curves to the 6 data points, and the resulting parameters are provided in Tables S6.1 and S6.2. Using these values in equation (4), the gradient of the tangent at a specific point was used to derive the activation energy, and consecutively plot the activation energy as function of ΔT for the non-milled powder and milled particulate materials.

The Friedman plots of the non-milled W/VO_2 powder and the milled W/VO_2 particulate materials (milling energy = 2143 kWh·t^{-1}, 11000 kWh·t^{-1} and 17000 kWh·t^{-1}) show that $|E_A|$ increases steeply when the material's temperature approaches T_0 (Fig. 4a). $|E_A|$ decreases with ΔT for all samples (Fig. 4b). The inverse proportionality of E_A to $(\Delta T)^2$ confirms that the formation of new nuclei in the original phase is the rate determining step of the SPT. This is consistent with the change in crystal structure when switching from VO_2 (M) to VO_2 (R) and *vice versa*: the growth of newly formed nuclei merely requires a minor change in atomic coordination, and bulk crystal remodelling is not required. Consequently, the activation energy corresponds to the free energy barrier for forming a nucleus [48]. Since the free energy barrier for forming a nucleus is inversely proportional to $(\Delta T)^2$ (Equation (2)), the activation energy decreases steeply with increasing difference between the material's temperature and the critical temperature T_0. Furthermore, the switching kinetics are symmetric for the non-milled W/VO_2 powder and milled W/VO_2 nanoparticles up to a milling energy of 11000 kWh·t^{-1}. At a milling energy of 17000 kWh·t^{-1}, $|E_A|$ is higher for the SPT from W/VO_2 (M) to W/VO_2 (R), inducing a kinetic asymmetry. $|E_A|$ at $\Delta T = 2.5$ °C for the SPT from W/VO_2 (R) to W/VO_2 (M) decreases upon milling from 676 kJ mol^{-1} (0 kWh·t^{-1}, D90 = 24 μm) to 290 kJ mol^{-1} (17000 kWh·t^{-1}, D90 = 0.12 μm). This is similar to the previously reported results obtained for milled undoped VO_2 particulate materials as progressive milling decreased $|E_A|$ from 1610 kJ mol^{-1} to 381 kJ mol^{-1} (17000 kWh·t^{-1}) [40]. In contrast, for the SPT from W/VO_2 (M) to W/VO_2 (R) $|E_A|$ at ΔT = 2.5 °C decreases from 668 kJ mol^{-1} (0 kWh·t^{-1}, D90 = 24 μm) to 404 kJ mol^{-1} (2143 kWh·t^{-1}, D90 = 3.14 μm) but then increases to 502 kJ mol^{-1} (17000 kWh·t^{-1}, D90 = 0.12 μm) [40]. Although $|E_A|$ is higher for undoped than for W-doped VO_2 powder (1610 vs. 668 kJ mol^{-1}), $|E_A|$ of undoped and W-doped nanoparticles are in the same order of magnitude (381 vs. 404 kJ mol^{-1}). For undoped and W-doped VO_2 particulate materials, a similar kinetic asymmetry was observed [40].

3.3. Thermochromic laminates comprising milled W/VO_2 nanoparticles

A masterbatch comprising 1 wt-% W/VO_2 nanoparticles in PVB was obtained by mixing a solution of PVB in ethanol and a dispersion of W/VO_2 nanoparticles in IPA, followed by removal of the solvent mixture through evaporation at 50 °C under reduced pressure. Subsequently, this material was mixed with PVB and 3-GO in a micro-compounder to produce strands with varying W/VO_2 concentration. These strands were then used to produce thermochromic laminates in a hot press. The laminates consisted of two glass plates with a nanocomposite thermochromic film as interlayer. For each of the milled W/VO_2 nanoparticle batches (2143, 11000 and 17000 kWh·t^{-1}), 5 laminates with different concentrations of nanoparticles in the PVB interlayer – ranging from 0.005 wt-% to 0.080 wt-% – were produced (SI8, SI9 and SI10). Using this lamination technique, precise control of the interlayer thickness was not feasible. For each laminate, we determined the individual interlayer thickness using a mitutoyo thickness gage. We selected three samples with similar W/VO_2 concentration (0.034 – 0.040 wt-%) and interlayer thickness (652 – 775 μm) for comparative analysis of T_{sol}, ΔT_{sol} and switching kinetics (Fig. 5, Table 3). With decreasing particle size obtained by progressive milling, T_{sol} increased from 61.6% (2143 kWh·t^{-1},

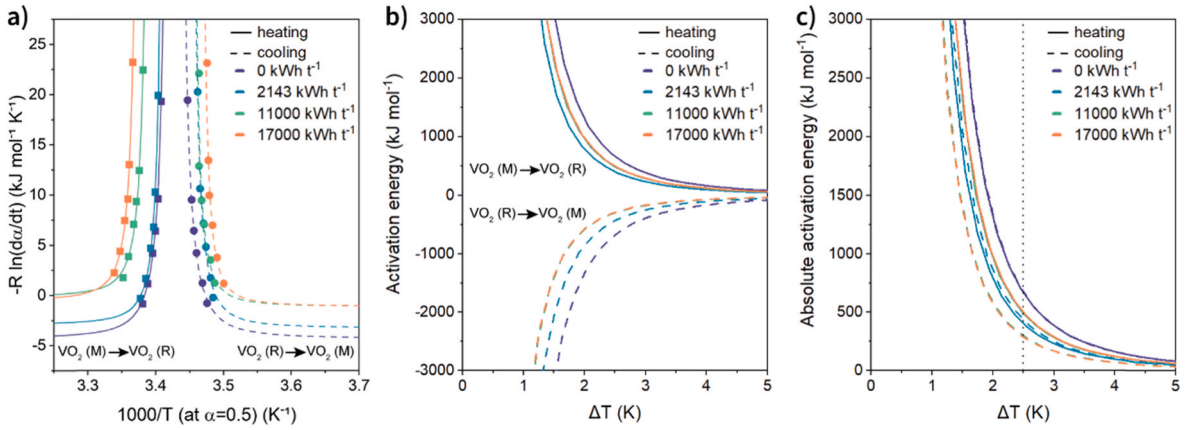

Fig. 4. a) Friedman plot for the non-milled powder and milled W/VO_2 particulate materials at $\alpha = 0.50$ for the VO_2 (M) to VO_2 (R) SPT and *vice versa*, b) activation energy of the non-milled powder and milled W/VO_2 particulate materials as function of ΔT, and c) absolute activation energy as function of ΔT for non-milled powder and milled W/VO_2 particulate materials.

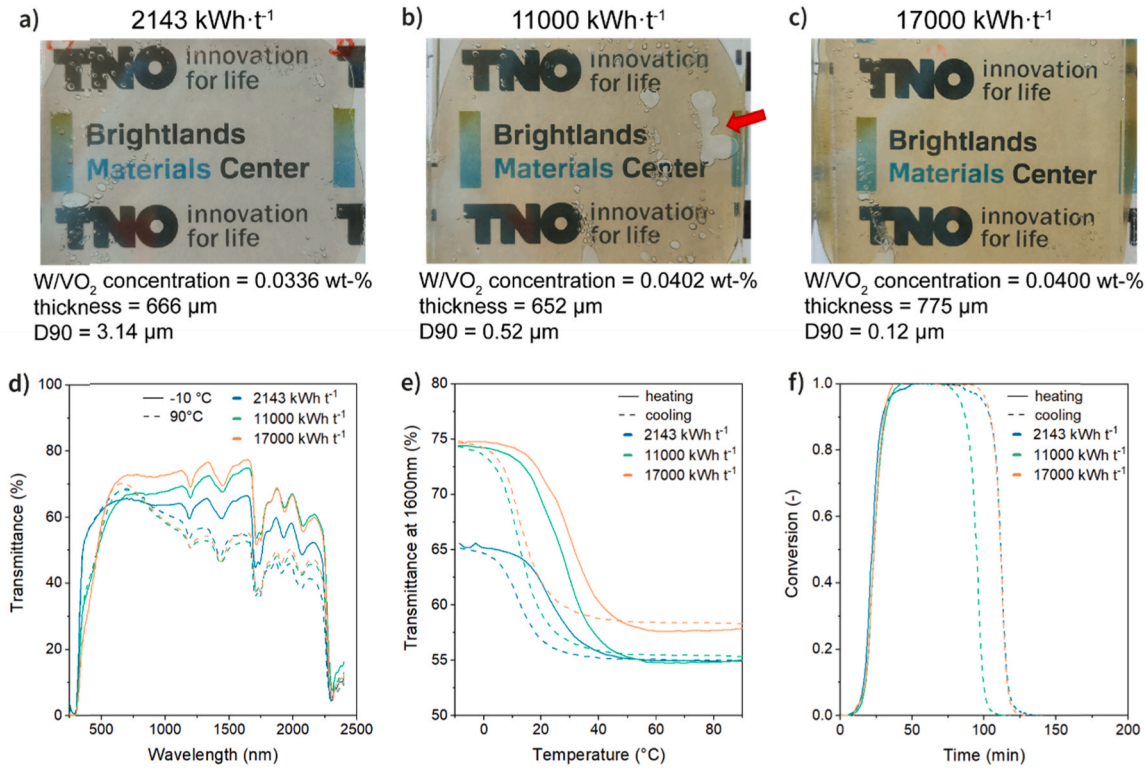

Fig. 5. Thermochromic laminate (pictures taken at room temperature (20 °C)) a) prepared from W/VO_2 particles obtained at a milling energy of 2143 kWh·t^{-1}, b) prepared from W/VO_2 particles obtained at a milling energy of 11000 kWh·t^{-1}, c) prepared from W/VO_2 particles obtained at a milling energy of 17000 kWh·t^{-1}, d) UV–vis–NIR transmission spectra measured at −10 °C and 90 °C for the thermochromic laminates, e) transmission at λ = 1600 nm of laminates as function of temperature upon heating and cooling with a rate of approximately 2 °C·min^{-1} and f) conversion-time profile derived from the measurements displayed in Fig. 5e. Note: air bubbles are included at some positions in the laminates as processing defects (example indicated with red arrow).

Table 3
Conversion rate for the W/VO_2 laminates and nanoparticles.

Bead milling energy input (kWh·t^{-1})	Laminate/ nanoparticles	W/VO_2 (M) to W/VO_2 (R)		W/VO_2 (R) to W/VO_2 (M)	
		Heating rate (°C·min^{-1})	Conversion rate (100 min^{-1})	Cooling rate (°C·min^{-1})	Conversion rate (100 min^{-1})
2143	laminate	2.0433	7.00	2.0016	10.65
11000		2.2457	7.57	2.1106	9.29
17000		1.9200	7.91	1.8635	10.14
2143	nanoparticles	1.5000	9.09	1.5000	8.71
11000			6.69		6.98
17000			6.12		6.18

D90 = 3.14 µm) to 61.8% (11000 kWh·t^{-1}, D90 = 0.52 µm) and 65.5% (17000 kWh·t^{-1}, D90 = 0.12 µm). Although ΔH decreased by more than 40% upon progressive milling (from 29.1 to 24.6 and 16.5 J g^{-1}), ΔT_{sol} increased from 1.4% (2143 kWh·t^{-1}) to 4.5% (11000 kWh·t^{-1}) and 7.7% (17000 kWh·t^{-1}). The main reason for this increase in T_{sol} and ΔT_{sol} with decreasing particle size is the reduction of Mie scattering (haze) in the cold state from 21.86% (2143 kWh·t^{-1}) to 12.19% (11000 kWh·t^{-1}) and 6.82% (17000 kWh·t^{-1}) (SI11). The switching rate of the thermochromic laminates was investigated by heating the samples from −10 °C to 90 °C and subsequently cooling them, both at a rate of approximately 2 °C·min^{-1}, and measuring the transmission at 1600 nm as a function of time and temperature. Then, the transmission as a function of temperature was converted into a conversion time profile (Fig. 5f), using a previously reported method [16]. The gradient between the conversion at α = 0.40 and α = 0.60 equals the switching rate (Table 3). The obtained switching rate was in the same order of magnitude as the values of the W/VO_2 nanoparticles obtained at a heating and cooling rate of 1.5 °C·min^{-1} (between 612 and 1065 min^{-1}, Table 3), which indicates that incorporation of W/VO_2 nanoparticles in PVB and subsequent lamination hardly affects their switching kinetics.

The optical properties, viz. T_{lum} and ΔT_{sol} of thermochromic laminates prepared with the smallest W/VO_2 nanoparticles produced in this study (D90 = 0.12 µm) were investigated using various W/VO_2 concentrations (Fig. 6a). The decrease in concentration from 0.0800 wt-% to 0.0051 wt-% resulted in an increase of T_{lum}, as expected, from 54.7% (0.0800 wt-%) to 82.5% (0.0051 wt-%) (Fig. 6a). At the same time, ΔT_{sol} decreased from 9.4% (0.0800 wt-%) to 3.5% (0.0051 wt-%) (Fig. 6c). For all concentrations, the laminates comprising the largest particles (D90 = 3.14 µm) display a reduced solar modulation compared to laminates with smaller particles (D90 = 0.52 µm and D90 = 0.12 µm, Fig. 6b), which is in agreement with the properties of the laminates reported above (Fig. 5). The solar modulation increases with increasing concentration of W/VO_2 nanoparticles while the T_{lum} remains similar with smaller particles (higher milling energy input). The ΔT_{sol} also increases with decreasing haze from 21.86% to 6.82% (SI11) which improves the overall properties of the thermochromic laminates. Of all laminates produced in this study, the highest ΔT_{sol} values were obtained with the smallest W/VO_2 nanoparticles (D90 = 0.12 µm). The highest

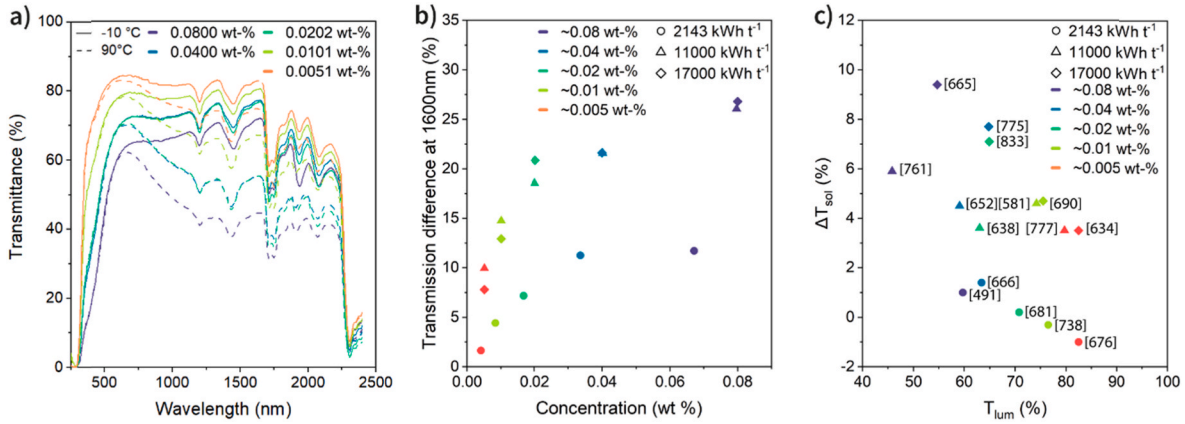

Fig. 6. a) UV–vis–NIR transmission spectra measured at −10 °C and 90 °C for the thermochromic laminate comprising nanoparticles obtained at a milling energy of 17000 kWh^{-1} (D90 = 0.12 μm) at different W/VO_2 concentrations, b) difference in transmission at 1600 nm for the thermochromic laminates with different W/VO_2 particle size and concentration, c) overview of ΔT_{sol} versus T_{lum} for all thermochromic laminates produced for this study (value in brackets is film thickness in μm). The D90 sizes of the milled particles were 3.14 ± 0.08 μm (2143 $kWh{\cdot}t^{-1}$), 0.52 ± 0.03 μm (11000 $kWh{\cdot}t^{-1}$) and 0.12 ± 0.01 μm (17000 $kWh{\cdot}t^{-1}$).

ΔT_{sol} of 9.4% was obtained for a laminate of 665 μm thickness comprising 0.0800 wt-% of these particles.

Very recently, Yeung et al. provided an overview of the best reported thermochromic coatings and films. The glass laminate with the highest ΔT_{sol} of 9.4% achieved in this study displays a T_{lum} of 54.7% [20]. In Yeung's overview, this would be positioned in the range of best-in-class single layer VO_2-based thermochromic coatings [20]. To further improve the thermochromic properties of these laminates whilst retaining/improving their visible transparency, the size of the W/VO_2 nanoparticles needs to be further reduced to ≤100 nm since the haze value is rather high (6.82%), certainly when compared to the industrially accepted standard for laminated architectural glass (≤0.6%). Furthermore, process optimization is required, both for the powder production to avoid the formation of large W/VO_2 particles and consequently reduce the need for extensive milling, and the bead milling process itself to ensure efficient reduction of particle size to ≤100 nm with minimum loss in crystallinity and functional performance. After this optimization, the use of these particles is not solely limited to polymer films for glass lamination. They could also be applied in nanocomposite thermochromic coatings for application on glass (new smart windows) and polymer films (retrofit smart window application), and nanocomposite thermochromic polymer sheets such as polycarbonate for light-weight glazing applications.

STEM-EDX analysis of a representative thermochromic film

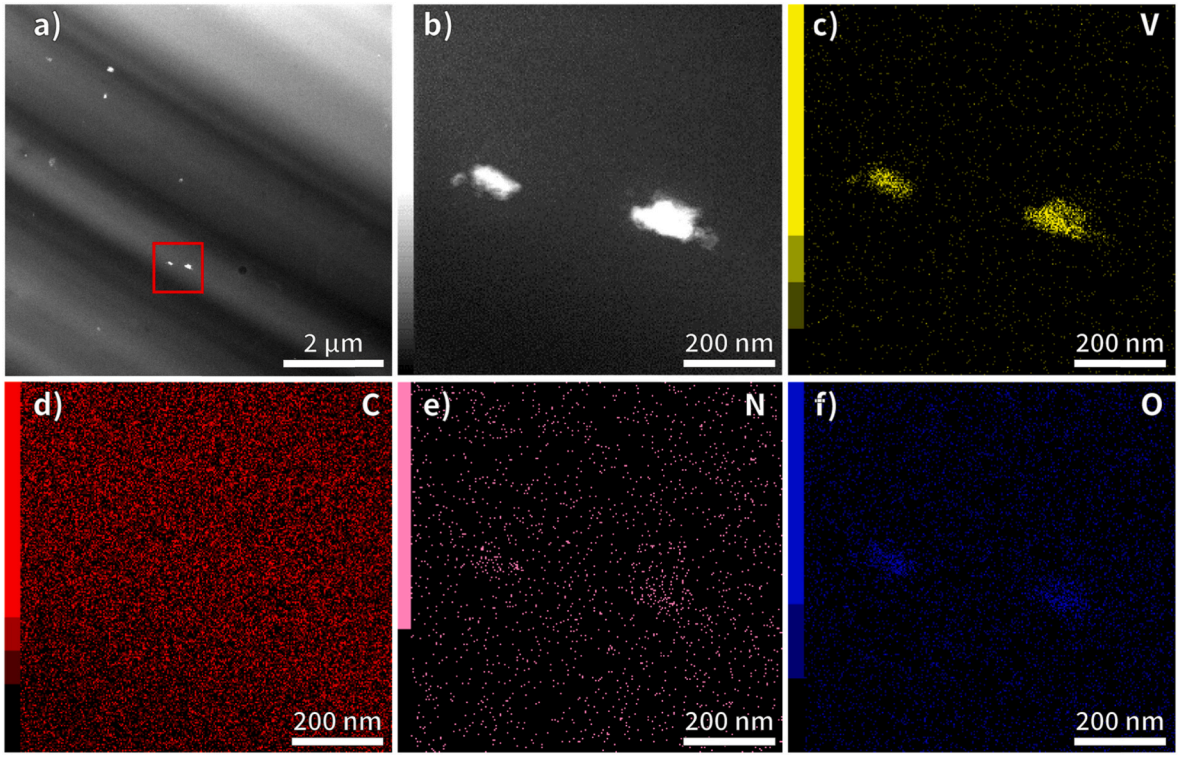

Fig. 7. STEM-EDX of thermochromic film comprising W/VO_2 (D90 = 0.12 μm, milling energy = 17000 $kWh{\cdot}t^{-1}$) at a concentration of 0.030 wt-% in PVB. a) HAADF-STEM image of a thermochromic film, red box indicates magnified region, b) HAADF-STEM magnified image of two particles in the thermochromic film, c) STEM-EDX map of elemental V, d) STEM-EDX map of elemental C, e) STEM-EDX map of elemental N, f) STEM-EDX map of elemental O (yellow: vanadium, red: carbon, pink: nitrogen and blue: oxygen).

consisting of W/VO_2 nanoparticles and PVB displayed W/VO_2 nanoparticles of a size below 200 nm randomly dispersed in the PVB matrix material (Fig. 7). The particle size is in good agreement with the particle size determined by SEM and laser diffraction (<400 nm and 120 nm, respectively). The nanoparticles included in the PVB film clearly comprise V and O as elements (Fig. 7c, f), and there seems to be a slight increase in the concentration of N at the position of the nanoparticles as well (Fig. 7e). Latter may be attributed to the N-containing PVP, which is used as surface modifier for the dispersion of W/VO_2 nanoparticles. However, this is difficult to unambiguously assign, due to the rather low concentration of PVP present in the film. The random dispersion of individual W/VO_2 nanoparticles clearly demonstrates that nanoparticle agglomeration does not occur during production and processing of the nanocomposite PVB film. Hence, the rather large haze value of the film (*vide supra*) is related to the size of the individual nanoparticles and not caused by clustering. Merely 0.14% of the area in the HAADF-STEM image (Fig. 7a) is occupied by W/VO_2 nanoparticles. This confirms the low concentration of W/VO_2 nanoparticles required to provide the PVB film with thermochromic properties that are of interest for smart glazing applications.

4. Conclusion

In conclusion we were able to synthesise high quality W-doped VO_2 powder using a chemical precursor synthesis followed by a multistep thermal anneal in a rotating tube furnace. The W/VO_2 powder displayed a switching enthalpy of 37.5 ± 0.2 J g^{-1} and a switching temperature between 17 and 20 °C. Subsequently, we successfully produced W/VO_2 nanoparticles by wet bead milling of this powder, and managed to reduce the particle size from 24 ± 2 μm to ultimately 120 ± 10 nm. We studied the thermodynamics and kinetics of differently sized W/VO_2 nanoparticles obtained in various stages of the bead milling process, and discovered a reduction in switching enthalpy upon progressive milling from 37.5 ± 0.2 J g^{-1} (non-milled powder) to ultimately 18.2 ± 0.6 J g^{-1} (milling energy = 17000 kWh·t^{-1}, particle size = 120 ± 10 nm). We attributed this to a partial loss in crystallinity. Furthermore, we noticed that the activation energy for the switch decreased upon milling, and that nanoparticles obtained at high milling energy displayed kinetic asymmetry with a faster switch from VO_2 (R) to VO_2 (M).

Integrating the W/VO_2 nanoparticles in PVB via a masterbatch and using the resulting thermochromic PVB for the production of laminated glass illustrated the potential of bead milled W/VO_2 nanoparticles for application in energy efficient thermochromic glazing. The switching kinetics of the thermochromic PVB laminates were in the same order of magnitude as for the respective W/VO_2 nanoparticles, as demonstrated by temperature-dependent UV–vis–NIR spectrophotometric analyses. The decrease of the particle size by progressive bead milling from 24 μm to 120 nm increases both ΔT_{sol} and T_{sol}. This increase in solar modulation is remarkable, since the switching enthalpy of W/VO_2 nanoparticles decreases upon progressive milling due to a partial loss of crystallinity. We mainly attributed this increase to a reduction in Mie scattering (haze) with decreasing particle size. Of all laminates produced in this study, the highest ΔT_{sol} values were obtained with the smallest W/VO_2 nanoparticles (D90 = 120 ± 10 nm). The highest ΔT_{sol} of 9.4% was obtained for a laminate of 665 μm thickness comprising 0.0800 wt-% of these particles.

The results of our study have a direct impact on the application of W/VO_2 nanoparticles and nanocomposite films in smart windows: they clearly demonstrate that even the smallest W/VO_2 nanoparticles (D90 = 120 ± 10 nm) integrated in PVB films scatter too much visible light, since the haze value of 6.82% is still significantly higher than the industrially accepted standard (≤0.6%). This implies that additional milling is required to further reduce the particle size, which will probably have a strong negative impact on the switching performance of the particles due to progressive loss in crystallinity and accompanying reduction in switching enthalpy. In future work, focus will be on improving the powder production to avoid the formation of large W/VO_2 particles and consequently reduce the need for extensive milling. Lastly the bead milling process itself will be optimized to ensure efficient reduction of particle size to ≤100 nm with minimum loss in crystallinity and functional performance. The kinetic characteristics of W/VO_2 nanoparticles and nanocomposite films are of key importance for fine-tuning of T_0 for the application in smart windows. To facilitate a switch at the temperature which is optimized for energy savings, T_0 should be set about 3 °C lower to ensure the switch is sufficiently fast at the temperature of choice. Because of the solar light absorption of the W/VO_2 nanoparticles and films, in practice photothermal heating may play an important role. Currently, we are investigating real-life performance and the impact of photothermal heating on the switching characteristics by monitoring the performance of a 1 m^2 sized demonstrator window comprising a W/VO_2-PVB thermochromic film in a test building in The Netherlands for 12 months, to obtain a complete insight into its behaviour over all 4 seasons.

CRediT authorship contribution statement

Lavinia Calvi: Writing – original draft, Visualization, Validation, Methodology, Investigation, Formal analysis, Data curation, Conceptualization. **Ryan van Zandvoort:** Writing – original draft, Visualization, Methodology, Investigation, Formal analysis, Data curation, Conceptualization. **Luc Leufkens:** Writing – original draft, Visualization, Investigation, Formal analysis, Data curation. **Janique F.B. Hupperetz:** Writing – original draft, Validation, Methodology, Investigation. **Roberto Habets:** Writing – review & editing, Methodology, Investigation, Formal analysis. **Daniel Mann:** Writing – review & editing, Supervision. **Nicole Meulendijks:** Writing – review & editing, Resources, Project administration, Investigation, Funding acquisition. **Marcel A. Verheijen:** Writing – review & editing, Visualization, Investigation, Formal analysis, Data curation. **Ken Elen:** Writing – review & editing, Supervision, Formal analysis, Data curation. **An Hardy:** Writing – review & editing, Supervision, Methodology, Conceptualization. **Marlies K. Van Bael:** Writing – review & editing, Supervision, Resources, Project administration, Funding acquisition, Conceptualization. **Pascal Buskens:** Writing – review & editing, Supervision, Resources, Methodology, Funding acquisition, Conceptualization.

Declaration of competing interest

The authors declare the following financial interests/personal relationships which may be considered as potential competing interests: Lavinia Calvi reports financial support was provided by NWO-SIA. Lavinia Calvi, Marlies K. Van Bael, An Hardy reports financial support was provided by Flemish Methusalem project. Pascal Buskens reports financial support was provided by Interreg Flanders-Netherlands. Marcel A. Verheijen reports financial support was provided by Solliance and Dutch Province of Noord-Brabant.

Data availability

Data will be made available on request.

Acknowledgements

The authors thank NWO-SIA (RAAK-PRO project Window of the Future) for their financial support as well as the Flemish Methusalem project NANO. The authors acknowledge financial support from the European Fund for Regional Development through the cross-border collaborative Interreg V program Flanders-The Netherlands (project SUNOVATE), co-financed by the Belgian province of Limburg and the Dutch provinces of Limburg and Noord-Brabant. Solliance and the Dutch province of Noord-Brabant are acknowledged for funding the TEM facility.

Appendix A. Supplementary data

Supplementary data to this article can be found online at https://doi.org/10.1016/j.solmat.2023.112350.

References

[1] W.-K. Hong, S. Cha, J.I. Sohn, J.M. Kim, Metal-insulator phase transition in quasi-one-dimensional VO_2 structures, J. Nanomater. 2015 (2015), https://doi.org/10.1155/2015/538954.

[2] A. Krammer, A. Matilainen, K. Pischow, A. Schüler, VO_2:Ge based thermochromic solar absorber coatings, Sol. Energy Mater. Sol. Cells 240 (2022), 111680, https://doi.org/10.1016/j.solmat.2022.111680.

[3] Z. Shao, X. Cao, H. Luo, P. Jin, Recent progress in the phase-transition mechanism and modulation of vanadium dioxide materials, NPG Asia Mater. 10 (7) (2018) 581–605, https://doi.org/10.1038/s41427-018-0061-2.

[4] Y. Cui, Y. Ke, C. Liu, Z. Chen, N. Wang, L. Zhang, Y. Zhou, S. Wang, Y. Gao, Y. Long, Thermochromic VO_2 for energy-efficient smart windows, Joule 2 (9) (2018) 1707–1746, https://doi.org/10.1016/j.joule.2018.06.018.

[5] J. Kim, T. Paik, Recent advances in fabrication of flexible, thermochromic vanadium dioxide films for smart windows, Nanomaterials 11 (10) (2021) 2674, https://doi.org/10.3390/nano11102674.

[6] Q. Chang, D. Wang, Z. Zhao, C. Ling, C. Wang, H. Jin, J. Li, Size-controllable M-phase VO_2 nanocrystals for flexible thermochromic energy-saving windows, ACS Appl. Nano Mater. 4 (7) (2021) 6778–6785, https://doi.org/10.1021/acsanm.1c00835.

[7] J. Schläefer, C. Sol, T. Li, D. Malarde, M. Portnoi, T.J. Macdonald, S.K. Laney, M. J. Powell, I. Top, I.P. Parkin, et al., Thermochromic VO_2 - SiO_2 nanocomposite smart window coatings with narrow phase transition hysteresis and transition gradient width, Sol. Energy Mater. Sol. Cells 200 (2019), 109944, https://doi.org/10.1016/j.solmat.2019.109944.

[8] S. Liu, C.Y. Tso, H.H. Lee, Y.W. Du, K.M. Yu, S.-P. Feng, B. Huang, Self-densified optically transparent VO_2 thermochromic wood film for smart windows, ACS Appl. Mater. Interfaces 13 (19) (2021) 22495–22504, https://doi.org/10.1021/acsami.1c03803.

[9] H. Zhang, H. Yu, Z. Chen, H. Luo, Y. Gao, Thermal kinetic analysis of metal–insulator transition mechanism in W-doped VO_2, J. Therm. Anal. Calorim. 126 (2) (2016) 949–957, https://doi.org/10.1007/s10973-016-5579-3.

[10] Y. Ji, A. Mattsson, G.A. Niklasson, C.G. Granqvist, L. Österlund, Synergistic TiO_2/VO_2 window coating with thermochromism, enhanced luminous transmittance, and photocatalytic activity, Joule 3 (10) (2019) 2457–2471, https://doi.org/10.1016/j.joule.2019.06.024.

[11] S.J. Lee, D.S. Choi, S.H. Kang, W.S. Yang, S. Nahm, S.H. Han, T. Kim, VO_2/WO_3-Based hybrid smart windows with thermochromic and electrochromic properties, ACS Sustain. Chem. Eng. 7 (7) (2019) 7111–7117, https://doi.org/10.1021/acssuschemeng.9b00052.

[12] M. Aburas, V. Soebarto, T. Williamson, R. Liang, H. Ebendorff-Heidepriem, Y. Wu, Thermochromic smart window technologies for building application: a review, Appl. Energy 255 (June) (2019), 113522, https://doi.org/10.1016/j.apenergy.2019.113522.

[13] C.G. Granqvist, Thermochromic VO2 for energy-efficient glazing: an introduction, in: Y. Long, Y. Gao (Eds.), Vanadium Dioxide-Based Thermochromic Smart Windows, Jenny Stanford Publishing, 2021, https://doi.org/10.1201/9781003177319.

[14] D. Mann, C. Yeung, R. Habets, Z. Vroon, P. Buskens, Comparative building energy simulation study of static and thermochromically adaptive energy-efficient glazing in various climate regions, Energies 13 (2020) 2842, https://doi.org/10.3390/en13112842.

[15] R. Tällberg, B.P. Jelle, R. Loonen, T. Gao, M. Hamdy, Comparison of the energy saving potential of adaptive and controllable smart windows: a state-of-the-art review and simulation studies of thermochromic, photochromic and electrochromic technologies, Sol. Energy Mater. Sol. Cells 200 (2019) 1–30, https://doi.org/10.1016/j.solmat.2019.02.041.

[16] L. Calvi, L. Leufkens, C.P.K. Yeung, R. Habets, D. Mann, K. Elen, A. Hardy, M. K. Van Bael, P. Buskens, A comparative study on the switching kinetics of W/VO_2 powders and VO_2 coatings and their implications for thermochromic glazing, Sol. Energy Mater. Sol. Cells 224 (2021) (2021), 110977, https://doi.org/10.1016/j.solmat.2021.110977.

[17] L. Chen, C. Huang, G. Xu, L. Miao, J. Shi, J. Zhou, X. Xiao, Synthesis of thermochromic W-doped VO_2 (M/R) nanopowders by a simple solution-based process, J. Nanomater. 2012 (2012) 1–8, https://doi.org/10.1155/2012/491051.

[18] J. Shi, S. Zhou, B. You, L. Wu, Preparation and thermochromic property of tungsten-doped vanadium dioxide particles, Sol. Energy Mater. Sol. Cells 91 (19) (2007) 1856–1862, https://doi.org/10.1016/j.solmat.2007.06.016.

[19] S.-Y. Li, G.A. Niklasson, C.G. Granqvist, Thermochromic fenestration with VO_2-based materials: three challenges and how they can Be met, Thin Solid Films 520 (2012) 3823–3828, https://doi.org/10.1016/j.tsf.2011.10.053.

[20] C.P.K. Yeung, R. Habets, L. Leufkens, F. Colberts, K. Stout, M. Verheijen, Z. Vroon, D. Mann, P. Buskens, Phase separation of VO_2 and SiO_2 on SiO_2-coated float glass yields robust thermochromic coating with unrivalled optical properties, Sol. Energy Mater. Sol. Cells 230 (June) (2021), 111238, https://doi.org/10.1016/j.solmat.2021.111238.

[21] C. Liu, X. Cao, A. Kamyshny, J.Y. Law, S. Magdassi, Y. Long, VO_2/Si-Al gel nanocomposite thermochromic smart foils: largely enhanced luminous transmittance and solar modulation, J. Colloid Interface Sci. 427 (2014) 49–53, https://doi.org/10.1016/j.jcis.2013.11.028.

[22] X. Lyu, A. Heßler, X. Wang, Y. Cao, L. Song, A. Ludwig, M. Wuttig, T. Taubner, Combining switchable phase-change materials and phase-transition materials for thermally regulated smart mid-infrared modulators, Adv. Opt. Mater. 9 (16) (2021) 1–8, https://doi.org/10.1002/adom.202100417.

[23] F. Ding, S. Zhong, S.I. Bozhevolnyi, Vanadium dioxide integrated metasurfaces with switchable functionalities at terahertz frequencies, Adv. Opt. Mater. 6 (9) (2018) 1–8, https://doi.org/10.1002/adom.201701204.

[24] C. Xu, G. Liu, M. Li, K. Li, Y. Luo, Y. Long, G. Li, Optical switching and nanothermochromic studies of VO_2 (M) nanoparticles prepared by mild thermolysis method, Mater. Des. 187 (2020), 108396, https://doi.org/10.1016/j.matdes.2019.108396.

[25] I. Top, R. Binions, C. Sol, I. Papakonstantinou, M. Holdynski, S. Gaiaschi, I. Abrahams, Improved thermochromic properties in bilayer films of VO_2 with ZnO, SnO_2 and WO_3 coatings for energy efficient glazing, J. Mater. Chem. C 6 (46) (2018) 12555–12565, https://doi.org/10.1039/c8tc04543g.

[26] V.P. Prasadam, N. Bahlawane, F. Mattelaer, G. Rampelberg, C. Detavernier, L. Fang, Y. Jiang, K. Martens, I.P. Parkin, I. Papakonstantinou, Atomic layer deposition of vanadium oxides: process and application review, Mater. Today Chem. 12 (2019) 396–423, https://doi.org/10.1016/j.mtchem.2019.03.004.

[27] C. Zhou, D. Li, Y. Tan, Y. Ke, S. Wang, Y. Zhou, G. Liu, S. Wu, J. Peng, A. Li, et al., 3D printed smart windows for adaptive solar modulations, Adv. Opt. Mater. 8 (11) (2020) 1–10, https://doi.org/10.1002/adom.202000013.

[28] B. Zhuang, Z. Dai, S. Pang, H. Xu, L. Sun, F. Ma, 3D ordered macroporous VO_2 thin films with an efficient thermochromic modulation capability for advanced smart windows, Adv. Opt. Mater. 7 (22) (2019) 1–9, https://doi.org/10.1002/adom.201900600.

[29] S.Y. Li, G.A. Niklasson, C.G. Granqvist, Nanothermochromics: calculations for VO_2 nanoparticles in dielectric hosts show much improved luminous transmittance and solar energy transmittance modulation, J. Appl. Phys. 108 (2010), 063525, https://doi.org/10.1063/1.3487980.

[30] S.Y. Li, G.A. Niklasson, C.G. Granqvist, Nanothermochromics with VO_2-based core-shell structures: calculated luminous and solar optical properties, J. Appl. Phys. 109 (2011), 113515, https://doi.org/10.1063/1.3592350.

[31] C. Wang, H. Xu, C. Wang, T. Liu, S. Yang, Y. Nie, X. Guo, X. Ma, X. Jiang, Preparation of VO_2 (M) nanoparticles with exemplary optical performance from VO_2 (B) nanobelts by ball milling, J. Alloys Compd. 877 (2021), 159888, https://doi.org/10.1016/j.jallcom.2021.159888.

[32] F.Z. Shu, F.F. Yu, R.W. Peng, Y.Y. Zhu, B. Xiong, R.H. Fan, Z.H. Wang, Y. Liu, M. Wang, Dynamic plasmonic color generation based on phase transition of vanadium dioxide, Adv. Opt. Mater. 6 (7) (2018) 1–10, https://doi.org/10.1002/adom.201700939.

[33] F. Wang, H. Chen, D. Lan, F. Zhang, Y. Sun, X. Zhang, S. Li, T. Cheng, Highly efficient and robust broadband nano-VO_2(M) saturable absorber for nonlinear optics and ultrafast photonics, Adv. Opt. Mater. 9 (21) (2021) 1–8, https://doi.org/10.1002/adom.202100795.

[34] J.L. Victor, M. Gaudon, N. Penin, A. Chiron, U.C. Chung, O. Viraphong, A. Rougier, Innovative sintering process for fabrication of thermochromic smooth VO_2 ceramics, J. Alloys Compd. 890 (2021), 161890, https://doi.org/10.1016/j.jallcom.2021.161890.

[35] D. Mann, C. Yeung, R. Habets, R. Van Zandvoort, L. Leufkens, J. Hupperetz, D. Out, R. Valckenborg, Z. Vroon, P. Buskens, SunSmart – the first affordable, energy optimized smart window, IOP Conf. Ser. Earth Environ. Sci. 1085 (1) (2022), 012060, https://doi.org/10.1088/1755-1315/1085/1/012060.

[36] D. Mann, C. Yeung, R. Habets, Z. Vroon, P. Buskens, Building energy simulations for different building types equipped with a high performance thermochromic smart window, IOP Conf. Ser. Earth Environ. Sci. 855 (1) (2021), 012001, https://doi.org/10.1088/1755-1315/855/1/012001.

[37] Y. Lu, S. Zhou, G. Gu, L. Wu, Preparation of transparent, hard thermochromic polysiloxane/tungsten-doped vanadium dioxide nanocomposite coatings at ambient temperature, Thin Solid Films 534 (2013) 231–237, https://doi.org/10.1016/j.tsf.2013.02.130.

[38] C. Takai, M. Senna, S. Hoshino, H. Razavi-Khosroshahi, M. Fuji, Chemical and thermal properties of VO_2 mechanochemically derived from V_2O_5 by Co-milling with paraffin wax, RSC Adv. 8 (2018) 21306–21315, https://doi.org/10.1039/C8RA02159G.

[39] C. Wang, H. Xu, T. Liu, S. Yang, Y. Nie, C. Wang, X. Guo, B. Wang, X. Ma, X. Jiang, One-step ball milling synthesis of VO_2 (M) nanoparticles with exemplary thermochromic performance, SN Appl. Sci. 3 (436) (2021), https://doi.org/10.1007/s42452-021-04154-x.

[40] L. Calvi, R. van Geijn, L. Leufkens, R. Habets, K.L. Gurunatha, K. Stout, D. Mann, I. Papakonstantinou, I.P. Parkin, K. Elen, et al., The impact of bead milling on the thermodynamics and kinetics of the structural phase transition of VO_2 particulate materials and their potential for use in thermochromic glazing, Sol. Energy Mater. Sol. Cells 242 (April) (2022), 111783, https://doi.org/10.1016/j.solmat.2022.111783.

[41] R. Chhabra, M.G. Basavaraj (Eds.), Coulson and Richardson's Chemical Engineering Volume 2A: Particulate Systems and Particle Technology, sixth ed., Butterworth-Heinemann, 2019.

[42] M.E.A. Warwick, I. Ridley, R. Binions, The effect of variation in the transition hysteresis width and gradient in thermochromic glazing systems, Sol. Energy Mater. Sol. Cells 140 (2015) 253–265, https://doi.org/10.1016/j.solmat.2015.04.022.

[43] M. Warwick, I. Ridley, R. Binions, Variation of thermochromic glazing systems transition temperature, hysteresis gradient and width effect on energy efficiency, Buildings 6 (2) (2016) 22, https://doi.org/10.3390/buildings6020022.
[44] X. Xiao, H. Zhang, G. Chai, Y. Sun, T. Yang, H. Cheng, L. Chen, L. Miao, G. Xu, A cost-effective process to prepare VO_2 (M) powder and films with superior thermochromic properties, Mater. Res. Bull. 51 (2014) 6–12, https://doi.org/10.1016/j.materresbull.2013.11.051.
[45] S. Vyazovkin, N. Sbirrazzuoli, Isoconversional kinetic analysis of thermally stimulated processes in polymers, Macromol. Rapid Commun. 27 (18) (2006) 1515–1532, https://doi.org/10.1002/marc.200600404.
[46] H.L. Friedman, New methods for evaluating kinetic parameters from thermal analysis data, Polym. Lett. 7 (1969) 41–46, https://doi.org/10.1002/pol.1969.110070109.
[47] S. Vyazovkin, Isoconversional Kinetics of Thermally Stimulated Processes, Springer, 2015.
[48] R. Farasat, S. Vyazovkin, Nanoconfined solid–solid transitions: attempt to separate the size and surface effects, J. Phys. Chem. C 119 (17) (2015) 9627–9636, https://doi.org/10.1021/acs.jpcc.5b01716.